

A time reversal algorithm in acoustic media with Dirac measure approximations

Élie Bretin* Carine Lucas† Yannick Privat‡

March 31, 2017

Abstract

This article is devoted to the study of a photoacoustic tomography model, where one is led to consider the solution of the acoustic wave equation with a source term writing as a separated variables function in time and space, whose temporal component is in some sense close to the derivative of the Dirac distribution at $t = 0$. This models a continuous wave laser illumination performed during a short interval of time. We introduce an algorithm for reconstructing the space component H of the source term from the measure of the solution recorded by sensors during a time T all along the boundary of a connected bounded domain. It is based at the same time on the introduction of an auxiliary equivalent Cauchy problem allowing to derive explicit reconstruction formula and then to use of a deconvolution procedure. Numerical simulations illustrate our approach. Finally, this algorithm is also extended to elasticity wave systems.

Contents

1	Introduction and motivations	1
2	Description of the algorithm	3
2.1	Strategy and main results	3
2.2	Some reminders about Green functions for the wave equation	5
3	Proofs of the main results	7
3.1	Proof of Theorem 2.1	7
3.2	Proof of Proposition 2.2	9
4	Numerics and practical implementation of the algorithm	10
4.1	Time reversal imaging and approximation	10
4.2	Description of the numerical scheme	11
4.3	Application to photoacoustic imaging	12
5	Generalization to elasticity wave operators	15
6	Comments and conclusion	17

1 Introduction and motivations

This article is motivated by some recent applications for medical imaging purposes, namely the so-called *photoacoustic tomography method*. The main idea of the photoacoustic effect is simple: the tissue to be

*CNRS UMR 5208, INSA de Lyon, Institut Camille Jordan, Université de Lyon, 20, avenue Albert Einstein, 69621 Villeurbanne Cedex, France (elie.bretin@insa-lyon.fr)

†Université d'Orléans, Labo. MAPMO, CNRS, UMR 6628, Fédération Denis Poisson, FR 2964, Bat. Math., BP 6759, 45067 Orléans cedex 2, France (carine.lucas@univ-orleans.fr).

‡CNRS, Sorbonne Universités, UPMC Univ Paris 06, UMR 7598, Laboratoire Jacques-Louis Lions, F-75005, Paris, France (yannick.privat@upmc.fr).

imaged is usually irradiated by a nanosecond-pulsed laser at a given optical wavelength. This energy is converted into heat. Absorption of light by molecules beneath the surface creates a thermally induced pressure jump that propagates as a sound wave, which can be detected. By detecting the pressure waves, we can localize their heterogeneities (i.e., where light was absorbed) and obtain important information about the studied sample [2, 21, 39].

In the sequel, we chose to focus on the photoacoustic method but we mention a very similar hybrid imaging technic as for instance *thermoacoustic tomography* [38, 30, 31, 32] which is based on the generation of acoustic waves by illumination of a sample with a short electromagnetic pulse and for which the method investigated hereafter can be adapted.

In this work, we are not concerned with the quantitative part of the photoacoustic technique (see e.g. [10, 11, 16]).

A possible model is the following: let us denote by u_0 the pressure generated by the thermal expansion of tissues. Let Ω be a smooth bounded domain in \mathbb{R}^d with $d = 2, 3$. One considers the standard acoustic wave equation

$$\begin{cases} \partial_{tt}u_0(t, x) - \Delta u_0(t, x) = \frac{d\delta_0}{dt}H(x), & (t, x) \in \mathbb{R} \times \mathbb{R}^d, \\ u_0(t, x) = \partial_t u_0(t, x) = 0, & \forall t < 0, \end{cases} \quad (1.1)$$

where δ_0 stands for the Dirac measure with respect to the time variable t at $t = 0$ and $H \in L^2(\mathbb{R}^d, \mathbb{R})$ denotes the absorbed optical energy, in other words the initial source term resulting from the expansion of tissues [27, 37].

Notice that the presence of the derivative of the Dirac term at $t = 0$ denoted $\frac{d\delta_0}{dt}$, models a short pulsed illumination at $t = 0$. From a practical point of view, such a model appears not relevant in certain experimental situations, where (for instance) a continuous-wave laser illumination is performed during a short interval of time. In such a case, the right-hand-side in the p.d.e. model (1.1) has to be modified and leads to consider rather the equation

$$\begin{cases} \partial_{tt}u_\varepsilon(t, x) - \Delta u_\varepsilon(t, x) = \frac{df_\varepsilon}{dt}(t)H(x), & (t, x) \in \mathbb{R}^d \times \mathbb{R}, \\ u_\varepsilon(t, x) = \partial_t u_\varepsilon(t, x) = 0, & \forall t < -\varepsilon T_f, \end{cases} \quad (1.2)$$

where f_ε is defined for a small parameter $\varepsilon > 0$ by

$$f_\varepsilon(t) = \frac{1}{\varepsilon} f\left(\frac{t}{\varepsilon}\right), \quad (1.3)$$

and $f \in C^0(\mathbb{R})$ is a known excitation function whose support is included in $[-T_f, T_f]$ with $T_f > 0$. It is well-known that, with such a choice, the sequence of functions $(df_\varepsilon/dt)_{\varepsilon>0}$ converges to $d\delta_0/dt$ in the sense of distributions.

Furthermore, the source term $H(\cdot) \in L^2(\mathbb{R}^d)$ is assumed to have a support compactly included in a connected bounded domain Ω with $\text{dist}(\text{supp}(H), \partial\Omega) > 0$.

Let us introduce the function g_ε , standing for the information recorded by sensors on the boundary of Ω during a time T , defined by by

$$g_\varepsilon(t, y) = u_\varepsilon(t, y) \quad \text{for all } t \in [0, T] \text{ and } y \in \partial\Omega, \quad (1.4)$$

where T is supposed to be sufficiently large to satisfy $u_\varepsilon(t, \cdot) \simeq 0$ and $\partial_t u_\varepsilon(t, \cdot) \simeq 0$ in Ω , for every $t > T$ whenever $d = 2$ or $u_\varepsilon(t, \cdot) = \partial_t u_\varepsilon(t, \cdot) = 0$, for every $t > T$ whenever $d = 3$. Notice that the existence of such a time follows from the so-called Huyghens principle (see e.g. [23, Section 2.4]). The (imprecise) notation “ \simeq ” used above (for the sake of simplicity) will be commented at the beginning of Section 4 after.

The motivation of this work is to provide an algorithm allowing to reconstruct an approximation of the source term $H(\cdot)$ from the knowledge of the given data g_ε on $\partial\Omega \times [0, T]$.

In many application, the pulse is assumed to be a good approximation of the Dirac distribution derivative at $t = 0$, so that the model (1.1) appears relevant. In this setting, one can prove that the acoustic wave equation also solves the Cauchy problem

$$\begin{cases} \partial_{tt}u_0(t, x) - \Delta u_0(t, x) = 0, & (t, x) \in \mathbb{R}^d \times \mathbb{R}_+, \\ u_0(0, x) = H(x), \quad \partial_t u_0(0, x) = 0, & \text{for all } x \in \mathbb{R}^d. \end{cases} \quad (1.5)$$

In this framework, the linear inverse problem which consists to reconstruct H from given data g_0 as defined by (1.4), can then be easily solved by using for instance the time reversal algorithm [12, 4, 25, 29] or inversion formula such as the spherical Radon transform [6, 24, 33, 34, 35], or variational techniques [14]. In particular, an error estimate is derived in [28] which shows the stability of the time reversal imaging approach.

However, in many applications and typically when dealing with the photoacoustic tomography technique with a continuous pulse performed during a short time, the parameter ε is not small enough to replace the right-hand side by the term $d\delta_0/dt$, so that System (1.2) has to be considered instead of System (1.1). In such a case, the previous strategy cannot be used as well.

For instance, in the recent paper [17], the authors propose to correct the data g_ε by using a deconvolution algorithm associated to the kernel f_ε and then to apply the time reversal imaging on the corrected data. A difficulty of a such approach is that a deconvolution algorithm is always based on the regularity of the data and it is not the case of $g_{\varepsilon=0}$ even if the source H is smooth (see figure (6))

In this article, we introduce an alternative approach which consists to apply the classical time reversal imaging on the uncorrected data g_ε to obtain an approximation H_ε of the source H . We then explain how we can correct the effect of ε on H_ε by using a deconvolution algorithm where the kernel can be build explicitly and depends only on ε and f . One advantage of this new way is that a deconvolution algorithm on H_ε can be easily used as soon as the source H is sufficiently smooth.

The rest of the paper is organized as follows. The main results of this article including the complete description of the reconstruction algorithm are stated in Section 2.1. In section 2.2, we gather some tools including useful identities about the Green function Γ associated to the wave equation. The proofs of the main results are postponed to Section 3.2. Finally, we provide in Section 4 some numerical illustrations highlighting the potential of our approach.

2 Description of the algorithm

2.1 Strategy and main results

The key point of the algorithm we will introduce rests upon the introduction of an *equivalent Cauchy problem* of the form

$$\begin{cases} \partial_{tt}v_\varepsilon(t, x) - \Delta v_\varepsilon(t, x) = 0, & (t, x) \in \mathbb{R}^d \times \mathbb{R}_+, \\ v_\varepsilon(0, x) = H_\varepsilon(x), \quad \partial_t v_\varepsilon(0, x) = G_\varepsilon(x), & x \in \mathbb{R}^d, \end{cases} \quad (2.1)$$

the wording *equivalent* meaning that

$$g_\varepsilon(t, y) = u_\varepsilon(t, y) = v_\varepsilon(t, y), \quad \text{for all } t > 0 \text{ and } y \in \partial\Omega.$$

In other words, the notion of equivalence of problems is related to the choice of domain Ω and means that the data recorded on the boundary $\partial\Omega$ by using (2.1) and (1.2) are the same.

In the sequel, we will assume that the support of the source H is included in a compact set K of Ω . Using that the support of f_ε is contained in $[-\varepsilon T_f, \varepsilon T_f]$, we will show the existence of an equivalent Cauchy problem provided that

$$4\varepsilon T_f \leq d_K, \quad \text{with} \quad \text{dist}(K, \partial\Omega) = d_K. \quad (2.2)$$

Under such assumptions, we will build two operators \mathcal{L}_1 and \mathcal{L}_2 such that

$$H_\varepsilon = \mathcal{L}_1[f_\varepsilon, H], \quad G_\varepsilon = \mathcal{L}_2[f_\varepsilon, H],$$

whose expression is fully explicit.

Then, the reconstruction procedure of the source term H from the data g_ε will then be performed into two steps:

Step 1. Knowing the pulse f_ε (approximating the Dirac measure $\delta_{t=0}$), determination of the source term H_ε in (2.1) from the knowledge of g by using an approach either based on a standard time reversal algorithm or a spherical radon transform. Notice that there is an abundant literature about the aforementioned methods. One refers for instance to [4, 6] for more explanations about them.

Step 2. Reconstruction of the source H from the knowledge of H_ε . In this view, we use a deconvolution algorithm combined with the knowledge of the operators \mathcal{L}_i , $i = 1, 2$ such that

$$H_\varepsilon = \mathcal{L}_1[f_\varepsilon, H], \quad G_\varepsilon = \mathcal{L}_2[f_\varepsilon, H].$$

In what follows, we will focus on Step 2, by providing an explicit reconstruction formula. For that purpose, we will use an explicit representation of the solution of (1.2) combined with the so-called time reversal principle to take advantage of the data measured by sensors, that is (1.4).

The whole procedure is illustrated on Figure 1 and described with more details at the end of this section.

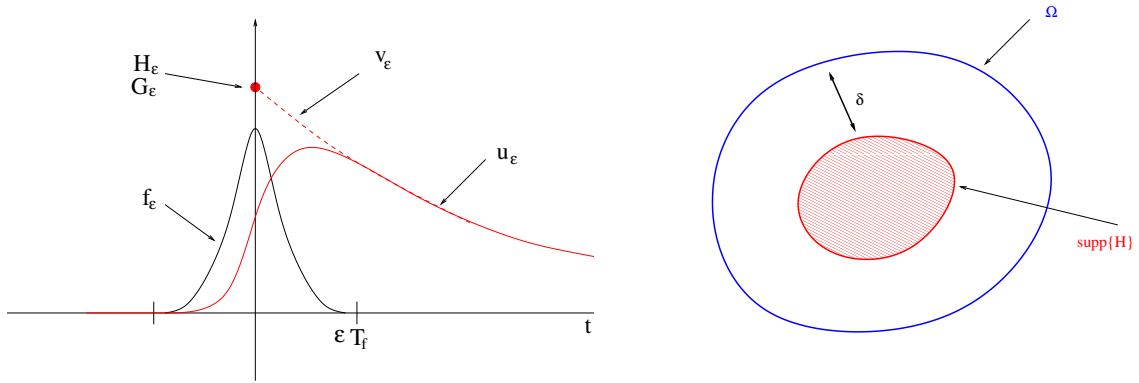


Figure 1: Principle of the time reversal approach

Notations. The following notations will be used throughout the paper.

- $\square := \partial_{tt} - \Delta$ (the d'Alembert operator);
- If $f : \mathbb{R} \rightarrow \mathbb{R}$ is a function, the notation f_o (resp. f_e) stand for the odd (resp. even) part of f ;
- For $x_0 \in \mathbb{R}^d$ (resp. $t_0 \in \mathbb{R}$), $\delta_{\{x=x_0\}}$ or simply δ_{x_0} when no confusion is possible (resp. $\delta_{\{t=t_0\}}$) denotes the Dirac distribution at $x = x_0$ (resp. at $t = t_0$).
- The operator \mathcal{F}_t (resp. \mathcal{F}_x) stands for the Fourier transform in time (resp. in space), in other words for every $H \in L^1(\mathbb{R}^d)$ and $f \in L^1(\mathbb{R})$, one has

$$\mathcal{F}_t[f] : \mathbb{R} \ni \omega \mapsto \int_{\mathbb{R}} f(t)e^{-it\omega} dt \quad \text{and} \quad \mathcal{F}_x[H] : \mathbb{R}^d \ni \xi \mapsto \int_{\mathbb{R}^d} H(x)e^{-ix \cdot \xi} dx.$$

- For S and T , two distributions having a compact support, the convolution product $S * T$ is defined (with obvious notations) by

$$\forall \varphi \in \mathcal{D}(\mathbb{R}^d), \quad \langle S * T, \varphi \rangle = \langle S_x \langle T_y, \varphi(x + y) \rangle \rangle.$$

- If X denotes a subset of \mathbb{R}^d , χ_X stands for the characteristic function of X , that is the function equal to 1 in X and 0 elsewhere.

Main result. The main result is related to the rewriting of the source terms H_ε and G_ε as convolution products of H by a kernel, namely

$$H_\varepsilon = H * K_{1,f_\varepsilon} \quad \text{and} \quad G_\varepsilon = H * K_{2,f_\varepsilon}$$

where the expression of the two kernels K_{1,f_ε} and K_{2,f_ε} is fully explicit (see Theorem 2.1 below).

Let us introduce the Green function Γ of the wave equation, namely the solution in a distributional sense of the Cauchy problem

$$\begin{cases} \partial_{tt}\Gamma(t, x) - \Delta\Gamma(t, x) = 0 & (t, x) \in \mathbb{R}^d \times \mathbb{R}_+, \\ \Gamma(0, \cdot) = 0, \quad \partial_t\Gamma(0, \cdot) = \delta_{\{x=0\}}. \end{cases} \quad (2.3)$$

Theorem 2.1. *Let $T_f > 0$, $\varepsilon > 0$, Ω be a connected bounded open set of \mathbb{R}^d and K be a compact set such that $K \subset \Omega$. If ε and K satisfy (2.2), then for all $H \in L^2(\mathbb{R}^d)$ such that $\text{supp}(H) \subset K$, there exists a Cauchy problem (2.1) equivalent to (1.2) in the sense made precise above. Moreover, H_ε and G_ε are given by*

$$H_\varepsilon = \mathcal{L}_1[f_\varepsilon, H] = H * K_{1,f_\varepsilon}, \quad \text{and} \quad G_\varepsilon = \mathcal{L}_2[f_\varepsilon, H] = H * K_{2,f_\varepsilon}.$$

where

$$K_{1,f_\varepsilon}(\cdot) = \int_{\mathbb{R}} f_\varepsilon(s) \partial_t \Gamma(s, \cdot) ds \quad \text{and} \quad K_{2,f_\varepsilon}(\cdot) = \int_{\mathbb{R}} f_\varepsilon(s) \partial_{tt} \Gamma(s, \cdot) ds,$$

Furthermore if $(f_\varepsilon)_{\varepsilon>0}$ converges to $\delta_{\{t=0\}}$ in the sense of distributions, then K_{1,f_ε} (resp. K_{2,f_ε}) converges to $\delta_{\{x=0\}}$ (resp. 0) in the sense of distributions.

The proof of this theorem is postponed to Section 3.2.

We complete the theorem above, by providing an explicit expression of the kernels K_{1,f_ε} and K_{2,f_ε} , which appears workable from a numerical point of view when performing all computations in the Fourier space.

Proposition 2.2. *Let $f \in L^2(\mathbb{R})$ be defined from its Fourier transform \hat{f} defined in \mathbb{R}^d by*

$$\hat{f}(\omega) = \sum_{n=0}^{+\infty} \alpha_n \omega^n, \quad \text{with } (\alpha_n)_{n \in \mathbb{N}} \in \ell^2(\mathbb{R}).$$

Then, one has

$$K_{1,f_\varepsilon}(x) = \mathcal{F}_x^{-1} \left[\hat{f}_e(|\xi|\varepsilon) \right] \quad \text{and} \quad K_{2,f_\varepsilon}(x) = i\mathcal{F}_x^{-1} \left[\frac{1}{|\xi|} \hat{f}_o(|\xi|\varepsilon) \right],$$

where f_e and f_o denote respectively the even and odd parts of f .

We derive from these results an algorithm that will be introduced and commented in Section 4.

2.2 Some reminders about Green functions for the wave equation

It is notable that Γ coincides with the solution in a distributional sense of the Cauchy problem

$$\begin{cases} \partial_{tt}\Gamma(t, x) - \Delta\Gamma(t, x) = \delta_{\{t=0\}} \delta_{\{x=0\}} & (t, x) \in \mathbb{R}^d \times \mathbb{R}_+, \\ \Gamma(t, \cdot) = \partial_t \Gamma(t, \cdot) = 0, & t < 0. \end{cases} \quad (2.4)$$

Lemma 2.3. *Let $T > 0$ and $F \in L^2(\mathbb{R}, L^2(\mathbb{R}^d))$ be such that $F(t, \cdot) = 0$ whenever $t < -T$. Then, the distributional solution U of $\square U = F$ such that $U = 0$ whenever $t < -T$ is*

$$U(t, \cdot) = \int_{\mathbb{R}} F(s, \cdot) * \Gamma(t - s, \cdot) ds \quad \forall t \geq -T,$$

where the convolution product $*$ operates between functions of the space variable x .

Notice that the temporal Green function $\Gamma(t, \cdot)$ can also be obtained as the inverse Fourier transform of Γ_ω

$$\Gamma(t, \cdot) = \mathcal{F}_t^{-1}[\Gamma_\omega(\cdot)](t),$$

where Γ_ω denotes the outgoing fundamental solution to the Helmholtz operator $-(\Delta + \omega^2)$ in \mathbb{R}^d , that is the distributional solution of the equation

$$(\Delta + \omega^2)\Gamma_\omega(x) = -\delta_{\{x=0\}} \quad x \in \mathbb{R}^d$$

subject to the outgoing Sommerfeld radiation equation

$$\lim_{|x| \rightarrow \infty} |x|^{\frac{d-1}{2}} \left(\frac{\partial}{\partial |x|} - ik \right) u(x) = 0$$

Lemma 2.4. *For $H \in L^2(\mathbb{R}^d)$ and $G \in H^{-1}(\mathbb{R}^d)$, if u solves in a distributional sense the wave equation*

$$\begin{cases} \partial_{tt}u(t, x) - \Delta u(t, x) = H(x) \frac{d\delta_{\{t=0\}}}{dt} + G(x)\delta_{\{t=0\}} & (t, x) \in \mathbb{R} \times \mathbb{R}^d, \\ u(t, \cdot) = \partial_t u(t, \cdot) = 0 & t < 0, \end{cases} \quad (2.5)$$

then, the restriction of u to positive times (still denoted by u with a slight abuse of notation) solves the p.d.e.

$$\begin{cases} \partial_{tt}u(t, x) - \Delta u(t, x) = 0 & (t, x) \in \mathbb{R}_+ \times \mathbb{R}^d, \\ u(0, \cdot) = H(\cdot), \quad \partial_t u(0, \cdot) = G(\cdot) \end{cases} \quad (2.6)$$

and there holds

$$\forall t \geq 0, \quad \begin{cases} u(t, \cdot) & = H * \partial_t \Gamma(t, \cdot) + G * \Gamma(t, \cdot) \\ \partial_t u(t, \cdot) & = H * \partial_{tt} \Gamma(t, \cdot) + G * \partial_t \Gamma(t, \cdot), \end{cases} \quad (2.7)$$

where the convolution product $*$ operates between functions of the space variable x .

Proof. Let Y denote the Heaviside step function. Let us denote temporarily by \tilde{u} the restriction of u to positive times, in other words $u = Y\tilde{u}$. Then, we get that \tilde{u} solves System (2.6) by plugging this expression into (2.5).

Let us show the first equality of (2.7), the second one being proved by similar arguments. Introduce the distribution $z = H * \partial_t \Gamma(t, \cdot)$. There holds

$$\begin{aligned} \square z(t, \cdot) &= \partial_{tt}(H * \partial_t \Gamma(t, \cdot)) - \Delta(H * \partial_t \Gamma(t, \cdot)) \\ &= H * \partial_{tt} \partial_t \Gamma(t, \cdot) - H * \Delta \partial_t \Gamma(t, \cdot) = H * \partial_t \square \Gamma(t, \cdot) \\ &= \frac{d\delta_{\{t=0\}}}{dt} H * \delta_{\{x=0\}} = \frac{d\delta_{\{t=0\}}}{dt} H. \end{aligned}$$

Therefore, z solves the main equation of (2.6) and one checks that $z(0, \cdot) = H(\cdot)$ and $\partial_t z(0, \cdot) = 0$. Mimicking this reasoning with the distribution $\tilde{z} = G * \Gamma(t, \cdot)$ yields that \tilde{z} solves the main equation of (2.6) and one checks that $\tilde{z}(0, \cdot) = 0$ and $\partial_t \tilde{z}(0, \cdot) = G(\cdot)$. By uniqueness of the solution of (2.6), we easily infer that $u = z + \tilde{z}$. \square

We then infer the following rewriting of the Green function Γ and its time derivative.

Proposition 2.5. *For all $t \in [0, s]$, there holds*

$$\begin{cases} \partial_t \Gamma(t, \cdot) & = \partial_t \Gamma(s-t, \cdot) * \partial_t \Gamma(s, \cdot) - \partial_{tt} \Gamma(t, \cdot) * \Gamma(s-t, \cdot) \\ \Gamma(t, \cdot) & = \Gamma(t, \cdot) * \partial_t \Gamma(s-t, \cdot) - \partial_t \Gamma(t, \cdot) * \Gamma(s-t, \cdot) \end{cases} \quad \text{in } \mathcal{D}'(\mathbb{R}^d).$$

In particular, considering $t = 0$, we obtain the identity:

$$\forall s > 0, \quad \delta_{\{x=0\}} = \partial_t \Gamma(s, \cdot) * \partial_t \Gamma(s, \cdot) - \partial_{tt} \Gamma(s, \cdot) * \Gamma(s, \cdot) \quad (2.8)$$

Proof. For all $s > 0$ and $t \in [0, s]$, the time reversal principle shows that the function v defined by $v(s, \cdot) = u(s - t, \cdot)$ solves the wave equation

$$\begin{cases} \partial_{tt}v(t, x) - \Delta v(t, x) = 0 & (t, x) \in [0, s] \times \mathbb{R}^d, \\ v(0, \cdot) = u(s, \cdot), \quad \partial_t v(0, \cdot) = \partial_t u(s, \cdot). \end{cases} \quad (2.9)$$

Let $t \in [0, s]$. According to Lemma 2.4, there holds

$$\begin{aligned} u(t, \cdot) &= v(s - t, \cdot) \\ &= u(s, \cdot) * \partial_t \Gamma(s - t, \cdot) - \partial_t u(s, \cdot) * \Gamma(s - t, \cdot) \\ &= (H * \partial_t \Gamma(s, \cdot) + G * \Gamma(s, \cdot)) * \partial_t \Gamma(s - t, \cdot) - (H * \partial_{tt} \Gamma(s, \cdot) + G * \partial_t \Gamma(s, \cdot)) * \Gamma(s - t, \cdot) \\ &= H * (\partial_t \Gamma(s - t, \cdot) * \partial_t \Gamma(s, \cdot) - \partial_{tt} \Gamma(s, \cdot) * \Gamma(s - t, \cdot)) \\ &\quad + G * (\Gamma(s, \cdot) * \partial_t \Gamma(s - t, \cdot) - \partial_t \Gamma(s, \cdot) * \Gamma(s - t, \cdot)) \end{aligned}$$

Moreover, since

$$u(t, \cdot) = H * \partial_t \Gamma(t, \cdot) + G * \Gamma(t, \cdot)$$

and since the functions H and G are arbitrary, we get the expected result. \square

In the sequel, it will be useful to use the following identities about Green's functions.

Proposition 2.6. *For all $p \in \mathbb{N}$, there holds*

$$\int_{\mathbb{R}} (-1)^p \omega^{2p} i \omega \Gamma_\omega(\cdot) d\omega = \Delta^p(\delta_{\{x=0\}}) \quad \text{and} \quad \int_{\mathbb{R}} (-1)^p \omega^{2p} \Gamma_\omega(\cdot) d\omega = 0.$$

Proof. According to Eq. (2.4), one has

$$\Gamma(\cdot, 0) = 0, \quad \text{and} \quad \partial_t \Gamma(\cdot, 0) = \delta_{\{x=0\}},$$

and by induction, we infer that

$$\forall n \in \mathbb{N}, \quad \frac{\partial^n \Gamma}{\partial t^n}(0, \cdot) = \begin{cases} \Delta^{(n-1)/2}(\delta_{\{x=0\}}), & \text{if } n \text{ is odd} \\ 0 & \text{if } n \text{ is even,} \end{cases}$$

where the distribution $\Delta^p(\delta_{\{x=0\}})$ is defined for $p \in \mathbb{N}^*$ by

$$\langle \Delta^p(\delta_{\{x=0\}}), \varphi \rangle = \Delta^p \varphi|_{\{x=0\}}, \quad \forall \varphi \in \mathcal{D}(\mathbb{R}^d).$$

The expected conclusion is obtained by reading these last identities in the Fourier space. \square

3 Proofs of the main results

3.1 Proof of Theorem 2.1

Equivalent Cauchy problem. Let us first introduce the solution w_ε of the acoustic wave equation

$$\begin{cases} \partial_{tt}w_\varepsilon(t, x) - \Delta w_\varepsilon(t, x) = 0, & (t, x) \in [0, \varepsilon T_f] \times \mathbb{R}^d, \\ w_\varepsilon(0, x) = u_\varepsilon(\varepsilon T_f, x), \quad \partial_t w_\varepsilon(0, x) = -\partial_t u_\varepsilon(\varepsilon T_f, x), & x \in \mathbb{R}^d. \end{cases} \quad (3.1)$$

and consider H_ε and G_ε defined by

$$H_\varepsilon(\cdot) = w_\varepsilon(\varepsilon T_f, \cdot), \quad \text{and} \quad G_\varepsilon(\cdot) = -\partial_t w_\varepsilon(\varepsilon T_f, \cdot).$$

Let us show that such choices of H_ε and G_ε as initial data for System (2.1) yield an equivalent problem. First, according to the time reversal principle (illustrated on Figure 1), we have

$$u_\varepsilon(x, t) = v_\varepsilon(x, t), \quad \forall x \in \mathbb{R}^d,$$

for every $t \geq \varepsilon T_f$.

Since $2\varepsilon T_f < d_K$, we infer that

$$u_\varepsilon(t, y) = 0, \quad \forall (t, y) \in [0, \varepsilon T_f] \times \partial\Omega.$$

by using the finite time propagation property of the wave equation.

Moreover, using now that $4\varepsilon T_f < d_K$ and by (still) using the finite time propagation property of the wave equation, we get that

$$\text{dist}(\text{supp}(u_\varepsilon(\varepsilon T_f, \cdot)), \partial\Omega) \geq d_K - 2\varepsilon T_f, \quad \text{dist}(\text{supp}(\partial_t u_\varepsilon(\varepsilon T_f, \cdot)), \partial\Omega) \geq d_K - 2\varepsilon T_f,$$

and

$$\text{dist}(\text{supp}(H_\varepsilon), \partial\Omega) \geq d_K - 3\varepsilon T_f, \quad \text{dist}(\text{supp}(G_\varepsilon), \partial\Omega) \geq d_K - 3\varepsilon T_f.$$

This yields that

$$\text{dist}(\text{supp}(v_\varepsilon), \partial\Omega) \geq d_K - 3\varepsilon T_f - t,$$

for all $t \in [0, \varepsilon T_f]$ which means that

$$v_\varepsilon(t, y) = 0, \quad \forall (t, y) \in [0, \varepsilon T_f] \times \partial\Omega.$$

Finally, we have proved that

$$u_\varepsilon(t, y) = v_\varepsilon(t, y), \quad \forall (t, y) \in \mathbb{R}_+ \times \partial\Omega.$$

Expression of $\mathcal{L}_1[f_\varepsilon, H]$ and $\mathcal{L}_2[f_\varepsilon, H]$. Notice that the operator \mathcal{L}_1 can be also defined as

$$\mathcal{L}_1[f_\varepsilon, H] = H_\varepsilon = w_\varepsilon(\varepsilon T_f, \cdot),$$

According to Lemma 2.4, there holds

$$\mathcal{L}_1[f_\varepsilon, H] = u_\varepsilon(\varepsilon T_f, x) * \partial_t \Gamma(\varepsilon T_f, \cdot) - \partial_t u_\varepsilon(\varepsilon T_f, \cdot) * \Gamma(\varepsilon T_f, \cdot).$$

Moreover, by using Lemma 2.3, since u_ε solves the p.d.e. (1.2) (notice that there holds in particular $\square u_\varepsilon = 0$ as $t \geq \varepsilon T_f$), one has for all $t \geq \varepsilon T_f$,

$$u_\varepsilon(t, x) = H * \left(\int_{\mathbb{R}} f_\varepsilon(s) \partial_t \Gamma(t - s, \cdot) ds \right) \quad \text{and} \quad \partial_t u_\varepsilon(t, x) = H * \left(\int_{\mathbb{R}} f_\varepsilon(s) \partial_{tt} \Gamma(t - s, \cdot) ds \right).$$

Combining the two previous facts and using Proposition 2.5 yields

$$\begin{aligned} \mathcal{L}_1[f_\varepsilon, H] &= u_\varepsilon(\varepsilon T_f, \cdot) * \partial_t \Gamma(\varepsilon T_f, \cdot) - \partial_t u_\varepsilon(\varepsilon T_f, \cdot) * \Gamma(\varepsilon T_f, \cdot) \\ &= H * \left(\int_{\mathbb{R}} f_\varepsilon(s) (\partial_t \Gamma(\varepsilon T_f - s, \cdot) * \partial_t \Gamma(\varepsilon T_f, \cdot) - \partial_{tt} \Gamma(\varepsilon T_f - s, \cdot) * \Gamma(\varepsilon T_f, \cdot)) ds \right), \\ &= H * \left(\int_{\mathbb{R}} f_\varepsilon(s) \partial_t \Gamma(s, \cdot) ds \right). \end{aligned}$$

We then infer that the operator $\mathcal{L}_1[f_\varepsilon, H]$ is a Kernel operator, in other words that

$$\mathcal{L}_1[f_\varepsilon, H] = H * K_{1, f_\varepsilon},$$

where its associated kernel K_{1, f_ε} reads

$$K_{1, f_\varepsilon}(\cdot) = \int_{\mathbb{R}} f_\varepsilon(s) \partial_t \Gamma(s, \cdot) ds.$$

The derivation of the second operator \mathcal{L}_2 is similar. Indeed, one has

$$\mathcal{L}_2[f_\varepsilon, H] = G_\varepsilon = -\partial_t w_\varepsilon(x, \varepsilon T_f),$$

and

$$\begin{aligned}
\mathcal{L}_2[f_\varepsilon, H] &= \partial_t u_\varepsilon(\varepsilon T_f, \cdot) * \partial_t \Gamma(\varepsilon T_f, \cdot) - u_\varepsilon(\varepsilon T_f, x) * \partial_{tt} \Gamma(\varepsilon T_f, \cdot) \\
&= H * \left(\int_{\mathbb{R}} f_\varepsilon(s) [\partial_{tt} \Gamma(\varepsilon T_f - s, \cdot) * \partial_t \Gamma(\varepsilon T_f, \cdot) - \partial_t \Gamma(\varepsilon T_f - s, \cdot) * \partial_{tt} \Gamma(\varepsilon T_f, \cdot)] ds \right), \\
&= H * \int_{\mathbb{R}} f_\varepsilon(s) \partial_{tt} \Gamma(s, \cdot) ds,
\end{aligned}$$

which is a kernel operator associated to the kernel

$$K_{2, f_\varepsilon}(\cdot) = \int_{\mathbb{R}} f_\varepsilon(s) \partial_{tt} \Gamma(s, \cdot) ds.$$

It remains to investigate the convergence properties of the operators.

Distributional limit as $\varepsilon \rightarrow 0$. Notice also that if $f_\varepsilon \rightarrow \delta_{\{t=0\}}$ in $\mathcal{D}'(\mathbb{R}^d)$ as $\varepsilon \rightarrow 0$, then for all $H \in L^2(\mathbb{R}^d)$ there holds

$$\lim_{\varepsilon \rightarrow 0} \mathcal{L}_1[f_\varepsilon, H] = \lim_{\varepsilon \rightarrow 0} H * \left(\int_{\mathbb{R}} f_\varepsilon(s) \partial_t \Gamma(\cdot, s) ds \right) = H * \partial_t \Gamma(0, \cdot) = H * \delta_{\{x=0\}} = H$$

by continuity of the convolution product. Similarly, one has also

$$\lim_{\varepsilon \rightarrow 0} \mathcal{L}_2[f_\varepsilon, H] = \lim_{\varepsilon \rightarrow 0} H * \left(\int_{\mathbb{R}} f_\varepsilon(s) \partial_{tt} \Gamma(s, \cdot) ds \right) = H * \partial_{tt} \Gamma(0, \cdot) = 0.$$

3.2 Proof of Proposition 2.2

In this section, we provide workable and explicit expressions of the kernels K_{1, f_ε} and K_{2, f_ε} . We first start with the usual case of Gaussian functions and generalize then to pulses in $L^2(\mathbb{R})$.

Case of Gaussian functions. Let us assume that $f(t) = \frac{1}{4\pi} \exp(-\frac{t^2}{4})$. Then its Fourier transform \hat{f} writes $\hat{f}(\omega) = \exp(-\omega^2)$ and the operator $\mathcal{L}_1[f_\varepsilon, H]$ can be identified from its kernel by

$$\begin{aligned}
K_{1, f_\varepsilon}(x) &= \int_{\mathbb{R}} f_\varepsilon(s) \partial_t \Gamma(s, x) ds = \int_{\mathbb{R}} \hat{f}(\varepsilon \omega) i \omega \Gamma_\omega(x) d\omega \\
&= \int_{\mathbb{R}} \sum_{p=0}^{+\infty} \frac{(-1)^p \varepsilon^{2p} \omega^{2p}}{p!} i \omega \Gamma_\omega(x) d\omega = \sum_{p=0}^{+\infty} \frac{(-\varepsilon^2 \Delta)^p}{p!} \delta_{\{x=0\}} \\
&= e^{-\varepsilon^2 \Delta} [\delta_{\{x=0\}}] = \mathcal{F}_x^{-1} \left[\frac{1}{(4\varepsilon\pi)^{d/2}} \exp\left(-\frac{\xi^2}{4\varepsilon^2}\right) \right] (x) = \mathcal{F}_x^{-1} \left[\frac{1}{\varepsilon} f\left(\frac{\xi}{\varepsilon}\right) \right] (x).
\end{aligned}$$

according to Proposition 2.6.

On the other side, the kernel associate to $\mathcal{L}_2[f_\varepsilon, H]$ vanishes since f is even. Indeed, it holds

$$K_{2, f_\varepsilon}(x) = \int_{\mathbb{R}} f_\varepsilon(s) \partial_{tt} \Gamma(s, x) ds = - \int_{\mathbb{R}} \hat{f}(\varepsilon \omega) \omega^2 \Gamma_\omega(x) d\omega = 0.$$

Case of a general pulse f . According to the decomposition of f in terms of its odd and even parts, to get the expected result, it is enough to consider the case where f is odd or even.

Let us assume that f is even and that its Fourier transform writes

$$\hat{f}(\omega) = \sum_{p=0}^{+\infty} \alpha_{2p} \omega^{2p}.$$

Then, one computes

$$\begin{aligned}
K_{1,f_\varepsilon}(x) &= \int_{\mathbb{R}} f_\varepsilon(s) \partial_t \Gamma(s, x) ds = \int_{\mathbb{R}} \hat{f}(\varepsilon \omega) i \omega \Gamma_\omega(x) d\omega \\
&= \int_{\mathbb{R}} \sum_{p=0}^{+\infty} (\alpha_{2p} \varepsilon^{2p} \omega^{2p}) i \omega \Gamma_\omega(x) d\omega = \sum_{p=0}^{+\infty} \alpha_{2p} (-\varepsilon^2 \Delta)^p \delta_{\{x=0\}} \\
&= \mathcal{F}_x^{-1} \left[\sum_{p=0}^{+\infty} \alpha_{2p} (\varepsilon^2 |\xi|^2)^p \right] = \mathcal{F}_x^{-1} \left[\hat{f}(|\xi| \varepsilon) \right]
\end{aligned}$$

and

$$K_{2,f_\varepsilon}(x) = \int_{\mathbb{R}} f_\varepsilon(s) \partial_{tt} \Gamma(s, x) ds = - \int_{\mathbb{R}} \hat{f}(\varepsilon \omega) \omega^2 \Gamma_\omega(x) d\omega = 0.$$

Let us now assume that f is odd, determined from its Fourier transform by

$$\hat{f}(\omega) = \sum_{p=0}^{+\infty} \alpha_{2p+1} \omega^{2p+1}.$$

Hence, one has

$$K_{1,f_\varepsilon}(x) = \int_{\mathbb{R}} f_\varepsilon(s) \partial_t \Gamma(s, x) ds = \int_{\mathbb{R}} \hat{f}(\varepsilon \omega) i \omega \Gamma_\omega(x) d\omega = 0$$

and

$$\begin{aligned}
K_{2,f_\varepsilon}(x) &= \int_{\mathbb{R}} f_\varepsilon(s) \partial_{tt} \Gamma(s, x) ds = - \int_{\mathbb{R}} \hat{f}(\varepsilon \omega) \omega^2 \Gamma_\omega(x) d\omega \\
&= i \int_{\mathbb{R}} \sum_{p=0}^{+\infty} (\alpha_{2p+1} \varepsilon^{2p+1} \omega^{2p}) i \omega \Gamma_\omega(x) d\omega = i \varepsilon \sum_{p=0}^{+\infty} \alpha_{2p+1} (-\varepsilon^2 \Delta)^p \delta_{\{x=0\}} \\
&= i \mathcal{F}_x^{-1} \left[\sum_{p=0}^{+\infty} \frac{1}{\xi^2} \alpha_{2p+1} (\varepsilon |\xi|)^{2p+1} \right] = i \mathcal{F}_x^{-1} \left[\frac{1}{|\xi|} \hat{f}(|\xi| \varepsilon) \right].
\end{aligned}$$

Combining the two last computations, one infers the desired result.

4 Numerics and practical implementation of the algorithm

This section is devoted to the presentation of numerical experiments highlighting the potential and the efficiency of our approach. All the numerical illustrations hereafter are restricted to the case $d = 2$. In that case, according to the Huyghens principle, we know that there does not exist a time T such that $u(t, \cdot) = \partial_t u(t, \cdot)$ for all $t > T$, where u_ε is the solution of (1.2). However, for each tolerance parameter $\eta > 0$, there exists $T_\eta > 0$ such that $\sup_{t > T_\eta} (\|u_\varepsilon(t, \cdot)\|_{L^\infty(\Omega)} + \|\partial_t u_\varepsilon(t, \cdot)\|_{L^\infty(\Omega)}) \leq \eta$. By using standard continuity results on the wave operator, one can show that, provided that η be small enough (and then that T_η be large enough), the initial data $H_{\varepsilon, \eta}$ and $G_{\varepsilon, \eta}$ reconstructed by using the time reversal principal are as close as wanted to H_ε and G_ε (see [28]). This remark legitimates the use of the aforementioned algorithm, even in the case of even dimensions of space.

4.1 Time reversal imaging and approximation

Recall that in the case where the source term is $f_0 = \delta_{\{t=0\}}$, the function u_0 satisfies

$$\begin{cases} \partial_{tt} u_0(t, x) - \Delta u_0(t, x) = 0, & (t, x) \in \mathbb{R}^d \times \mathbb{R}_+, \\ u_0(0, x) = H(x), \quad \partial_t u_0(0, x) = 0, & x \in \mathbb{R}^d. \end{cases} \quad (4.1)$$

and the observed data g_0 are defined by

$$g_0(t, y) = u_0(t, y) \quad \text{for all } (t, y) \in [0, T] \times \partial\Omega.$$

Then the reconstruction of the source term H from g_0 can be obtained by noting that

$$H(\cdot) = w(T, \cdot),$$

where w solves the wave equation

$$\begin{cases} \partial_{tt}w(t, x) - \Delta w(t, x) = 0, & (t, x) \in [0, T] \times \Omega, \\ w(0, x) = \partial_t w(0, x) = 0, & x \in \Omega, \\ w(t, y) = g_0(T - t, y), & (t, y) \in [0, T] \times \partial\Omega. \end{cases}$$

As commented in [4], the discretization of this imaging functional requires to interpolate the data on the boundary of Ω which generates smoothing effects on the reconstructed image. From a practical point of view, it is more efficient to use an approximation version of $H(\cdot)$ reading as

$$\mathcal{I}[g_0](x) = \int_0^T v_s(t, x) dx,$$

where v_s solves the wave equation

$$\begin{cases} \partial_{tt}^2 v_s(t, x) - \Delta v_s(t, x) = \partial_t (\delta_{\{t=s\}} g(x, T - s)) \delta_{\partial\Omega}, & (t, x) \in \mathbb{R}^d \times \mathbb{R} \\ v_s(t, x) = 0, \quad \partial_t v_s(t, x) = 0, & x \in \mathbb{R}^d, t < s. \end{cases}$$

Here, $\delta_{\{t=s\}}$ denotes the time Dirac distribution at time $t = s$ and $\delta_{\partial\Omega}$ is the surface Dirac measure on the manifold $\partial\Omega$.

In particular, by using the so-called Helmholtz-Kirchhoff identity¹, it is proved in [1] that when Ω is close to a sphere in \mathbb{R}^d with large radius, there holds

$$H(\cdot) \simeq \mathcal{I}[g_0](\cdot).$$

4.2 Description of the numerical scheme

The wave equations involved in the algorithm are solved in the box $Q = [-L/2, L/2]^2$ with periodic boundary conditions, where the size L is assumed to be sufficiently large to prevent any reflection on the boundary. Numerical integrations of each equation are then performed exactly in the Fourier space. Let us provide some precisions on them.

Fourier space discretization. Recall that the N -Fourier approximation of a $2D$ function u in a box $Q = [-L/2, L/2]^2$ is given by

$$u^N(t, x) = \sum_{n_1, n_2 = -N/2}^N c_{\mathbf{n}}(t) e^{2i\pi \xi_{\mathbf{n}} \cdot x},$$

where $\mathbf{n} = (n_1, n_2)$ and $\xi_{\mathbf{n}} = (n_1/L, n_2/L)$. Here the coefficient $c_{\mathbf{n}}$ represents the N^2 first discrete Fourier coefficients of u . Moreover, the inverse discrete Fourier transform of $c_{\mathbf{n}}$ allows to write that $u_{\mathbf{n}}^N = IFFT[c_{\mathbf{n}}]$ where $u_{\mathbf{n}}^N = u(x_{\mathbf{n}})$ denotes the value of the function u at the point $x_{\mathbf{n}} = (n_1 h_1, n_2 h_2)$ where $h_{\alpha} = L_{\alpha}/N$ for $\alpha \in \{1, 2\}$.

Conversely, $c_{\mathbf{n}}$ can be computed by applying the discrete Fourier transform to $u_{\mathbf{n}}^N$, namely

$$c_{\mathbf{n}} = FFT[u_{\mathbf{n}}^N].$$

¹Recall that, in a nutshell, this identity asserts that

$$\int_{\partial\Omega} \Gamma_{\omega}(x, y) \overline{\Gamma_{\omega}(x, z)} d\sigma(y) \simeq -\frac{i}{\omega} \text{Im} \Gamma(x, z),$$

for all x, z in \mathbb{R}^d , where Γ_{ω} denotes the outgoing fundamental solution to the Helmholtz operator.

Exact time integration We decide to approach the solution u of a generic wave equation

$$\partial_{tt}u(t, x) - \Delta u(t, x) = F(t, x) = \sum_{n_1, n_2 = -\infty}^{+\infty} f_{\mathbf{n}}(t) e^{2i\pi\xi_{\mathbf{n}} \cdot x} \quad \text{in } \mathbb{R} \times \mathbb{R}^d$$

completed by two initial conditions, by u^N , the solution of the “truncated system”

$$\partial_{tt}u^N(t, x) - \Delta u^N(t, x) = F^N(t, x) = \sum_{n_1, n_2 = -N}^N f_{\mathbf{n}}(t) e^{2i\pi\xi_{\mathbf{n}} \cdot x}$$

with two approximated initial conditions, which also reads

$$\frac{\partial}{\partial t} \begin{pmatrix} u^N \\ u_t^N \end{pmatrix} = \begin{pmatrix} 0 & I_d \\ \Delta & 0 \end{pmatrix} \begin{pmatrix} u^N \\ u_t^N \end{pmatrix} + \begin{pmatrix} 0 \\ F^N \end{pmatrix}.$$

The last system can be integrated coefficient by coefficient, by solving the $2N$ linear 2×2 systems of ordinary differential equations

$$\frac{d}{dt} \begin{pmatrix} c_{\mathbf{n}}(t) \\ c'_{\mathbf{n}}(t) \end{pmatrix} = \begin{pmatrix} 0 & 1 \\ -4\pi^2|\xi_{\mathbf{n}}|^2 & 0 \end{pmatrix} \begin{pmatrix} c_{\mathbf{n}}(t) \\ c'_{\mathbf{n}}(t) \end{pmatrix} + \begin{pmatrix} 0 \\ f_{\mathbf{n}}(t) \end{pmatrix}, \quad \text{for } \mathbf{n} = (n_1, n_2) \text{ and } n_i = -N, \dots, N, \quad i = 1, 2,$$

where $c'_{\mathbf{n}}(t) = \frac{dc_{\mathbf{n}}}{dt}(t)$. Notice that this system is simple enough to be solved explicitly.

4.3 Application to photoacoustic imaging

All the numerical simulations of this section are performed with the following set of parameters:

- Ω is a two-dimensional ball of radius 1 whose boundary is discretized by 2^{10} sensors,
- the box $Q = [-L/2, L/2]^d$ has size $L = 2$ and the record time is $T = 2$;
- we use a regular step discretization with parameters $dt = T/2^{10}$ and $dx = L/2^9$.

Time reversal Imaging using ideal data g_0 . On Figure 4.3, we use ideal data g_0 and as expected, one observes that the reconstructed source and the exact source are almost identical.

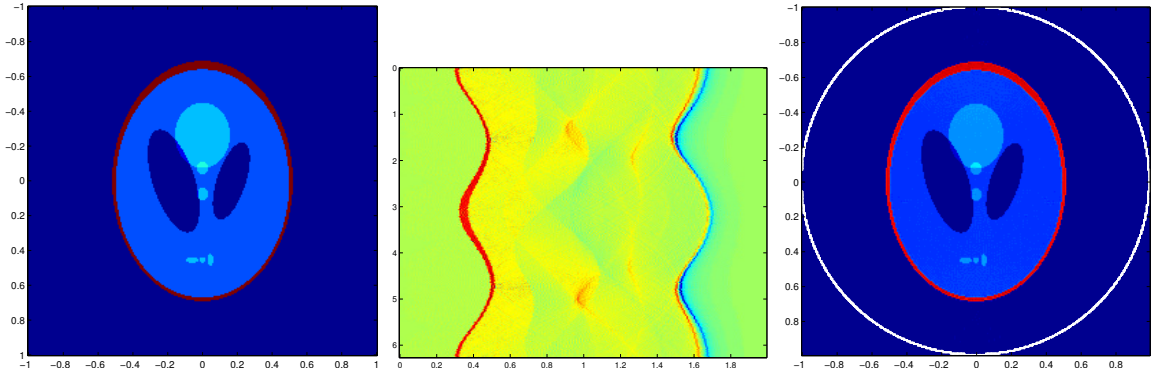


Figure 2: Source reconstruction using time reversal imaging \mathcal{I} ; Left - initial source H , middle - given data g , right - $\mathcal{I}[g]$

Time reversal Imaging using data g_ε . We now consider three different excitation functions f_1, f_2, f_3 (see Figure 4.3), defined by

$$\begin{aligned} f_1(t) &= \exp(-5\pi t^2) \\ f_2(t) &= \chi_{[-1/2, 1/2]}(t) \\ f_3(t) &= 3 * (\chi_{\{-0.6, -0.2, 0.2, 0.6\}} + \chi_{[-1/12, 1/12]})(t). \end{aligned}$$

On Figure 4, we observe the reconstructed source obtained by using the Imaging functional $\mathcal{I}[g_\varepsilon]$ with $\varepsilon = 0.1$.

The quality of the reconstruction does not seem not as good as in the case where $\varepsilon = 0$. Indeed, this is not surprising since the imaging functional $\mathcal{I}[g_\varepsilon]$ provides an efficient reconstruction of $H_\varepsilon = \mathcal{L}_1[f_\varepsilon, H]$, which can strongly differ from the source H whenever the coefficient ε is too large.

On Figure 6, the image of $H_\varepsilon = \mathcal{L}_1[f_\varepsilon, H]$ has been plotted and we observe that all the pictures correspond to the source imaging $\mathcal{I}[g_\varepsilon]$. This is a numerical illustration of the truthfulness of Theorem 2.1.

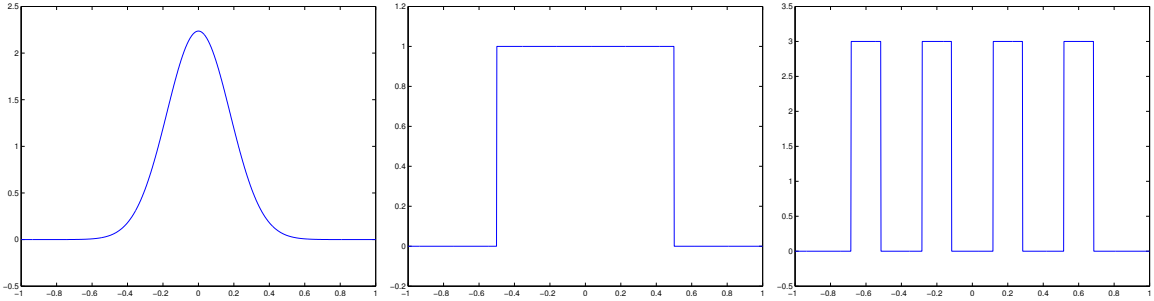


Figure 3: Plots of the three different excitation functions f_1, f_2 and f_3

Deconvolution algorithm by using a total variation regularization. In this last step of the algorithm, we reconstruct the source H from the numerical approximation $\tilde{H}_\varepsilon = \mathcal{I}[g_\varepsilon]$ by solving the optimization problem

$$H^* = \underset{H}{\operatorname{argmin}} J(H) \quad \text{with} \quad J(H) = \frac{1}{2} \int_{\Omega} (\mathcal{I}[g_\varepsilon] - K_{1, f_\varepsilon} * H)^2 + \gamma \int_{\Omega} |\nabla H| dx,$$

where γ is a (positive) regularization parameter. Nevertheless, a direct computation of H^* is sometimes difficult to implement because of the non-smooth character the Total Variation (TV) term. This is why we consider an approximation of H^* with the help of an iterative *shrinkage-thresholding* algorithm [22, 20]. This algorithm can be viewed as a splitting gradient descent iterative scheme:

- (0) *Initialization:* data g , initial solution $H_0 = 0$ are known,
- (1) *Data link step:* $H_{k+1/2} = H_k - \tau K_{1, f_\varepsilon} * [K_{1, f_\varepsilon} * H_k - \mathcal{I}[g_\varepsilon]]$,
- (2) *Regularization step:* $H_{k+1} = T_{\gamma\tau}[H_{k+1/2}]$,

where $\tau > 0$ is a virtual descent time step and the operator T_τ is defined by

$$T_\tau[u] = \underset{v}{\operatorname{argmin}} \left\{ \frac{1}{2} \|v - u\|_{L^2(\Omega)}^2 + \tau \|\nabla v\|_{L^1(\Omega)} \right\}.$$

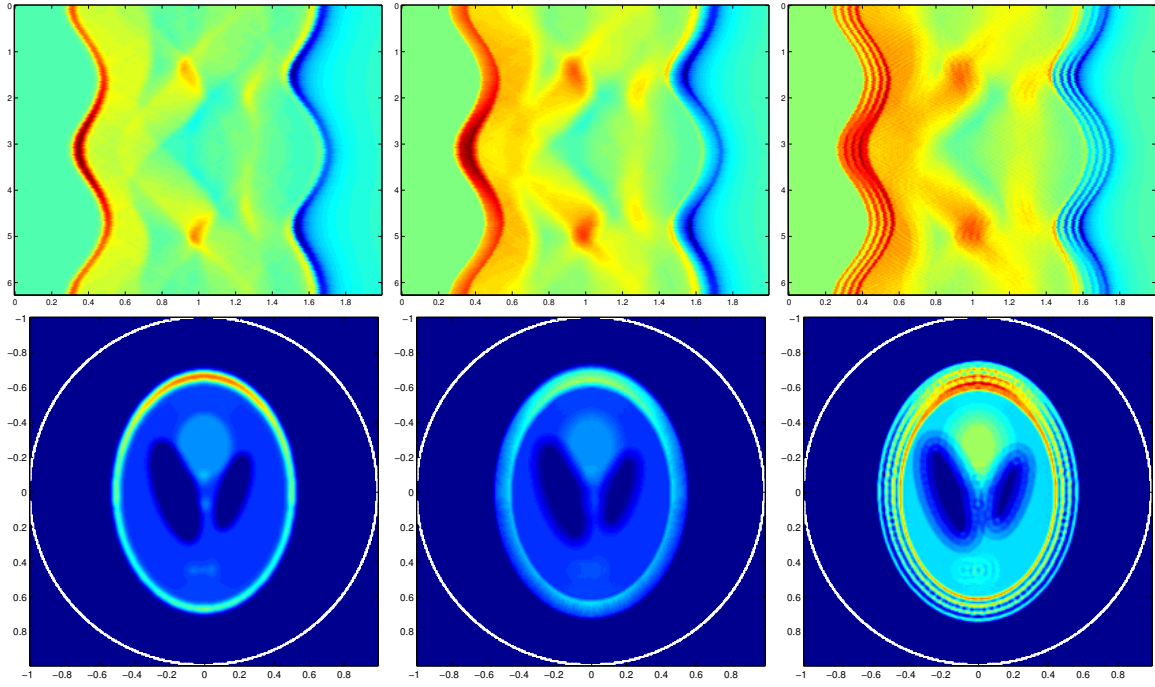


Figure 4: Time reversal imaging associated to the perturbed data g_ε ; First line : data g_ε ; second line : Imaging functional $\mathcal{I}[g_\varepsilon]$; Left to right: use of f_1, f_2 and f_3

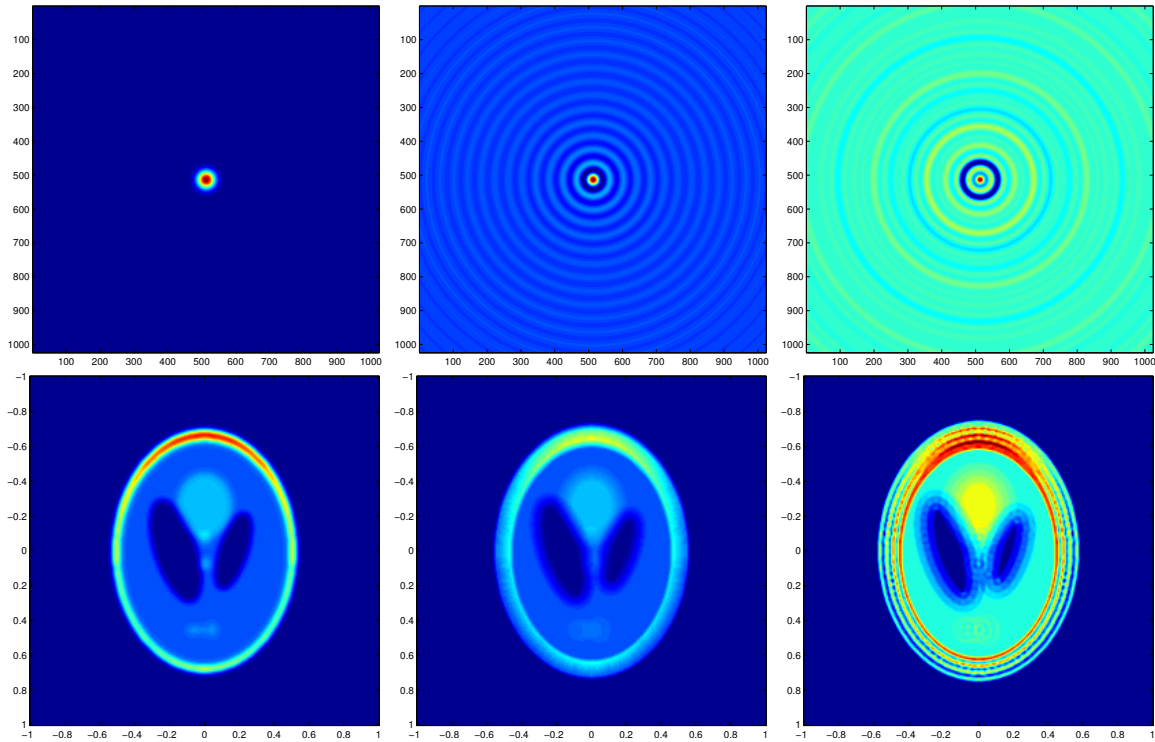


Figure 5: Kernel operator $\mathcal{L}_1[f_\varepsilon]$; First line : Spatial Fourier transform of the kernel K_{1,f_ε} ; Second line: $\mathcal{L}_1[f_\varepsilon][H] = H * K_{0,f_\varepsilon}$; Left to right: use of f_1, f_2 and f_3

The TV term is minimized implicitly by using the duality algorithm of Chambolle [19], which can be considered as an advantage of this approach. It is notable that this algorithm converges [22, 20] under a smallness assumption on the parameter τ , namely $\tau\|\mathcal{F}[K_{1,f_\varepsilon}]\|_\infty^2 \leq 1$. A possible variant consists in considering the algorithm by Beck and Teboulle [13] to accelerate the convergence rate. On Figure (4.3), the reconstructed source H^* obtained in the three different cases f_1 , f_2 and f_3 are plotted.

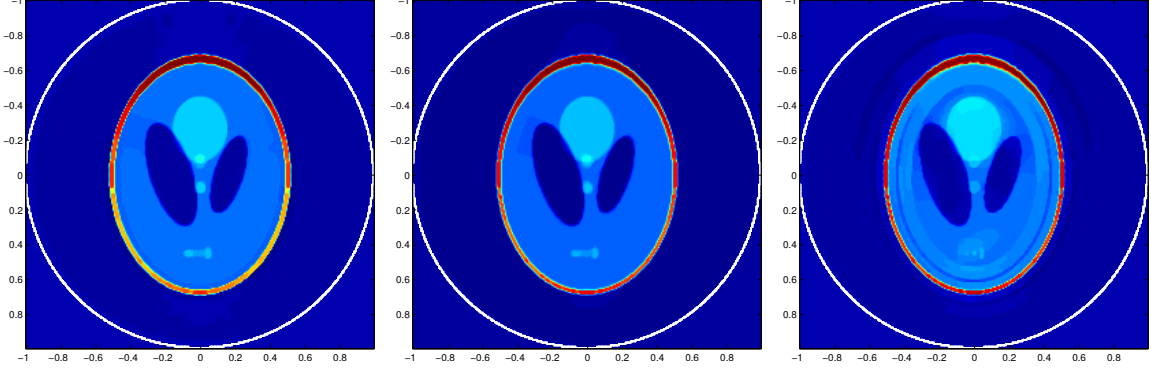


Figure 6: Correction of the source reconstruction using deconvolution algorithm with total variation regularization, Left to right : using f_1 , f_2 and f_3

5 Generalization to elasticity wave operators

The motivation of this section is to emphasize that our approach can be extended without special effort to many kinds of wave equation involving homogeneous operators in space. In particular, having in mind some recent advances on hybrid methods in biomedical imaging exploiting elastic properties of the soft tissue [8, 9, 7, 15, 26, 36], we focus on the linear elastic wave equation. For the sake of clarity and since all proofs follow exactly the same lines as those of Section 3.2, we will only provide the main steps allowing to extend our results in the framework of elastic waves.

Let us now consider the homogeneous isotropic elastic wave equation in a d -dimensional open medium

$$\begin{cases} \partial_t^2 \mathbf{u}_\varepsilon(x, t) - \mathcal{L}_{\lambda, \mu} \mathbf{u}_\varepsilon(x, t) = f'_\varepsilon(t) \mathbf{H}(x), & (x, t) \in \mathbb{R}^d \times \mathbb{R}, \\ \mathbf{u}_\varepsilon(x, t) = \partial_t \mathbf{u}_\varepsilon(x, t) = \mathbf{0}, & x \in \mathbb{R}^d, t < -\varepsilon T_f, \end{cases}$$

where

$$\mathcal{L}_{\lambda, \mu} \mathbf{u} = \mu \Delta \mathbf{u} + (\lambda + \mu) \nabla (\nabla \cdot \mathbf{u}).$$

Here (λ, μ) denote the Lamé coefficients of the medium. The inverse problem we consider here is to reconstruct the source \mathbf{H} from the data set

$$\left\{ \mathbf{g}_\varepsilon(y, t) = \mathbf{u}_\varepsilon(y, t), t \in [0, T], y \in \partial\Omega \right\},$$

Case of ideal data: $\varepsilon = 0$. In the ideal case with $\varepsilon = 0$, we are led to consider the function \mathbf{u}_0 solution of

$$\begin{cases} \partial_t^2 \mathbf{u}_0(x, t) - \mathcal{L}_{\lambda, \mu} \mathbf{u}_0(x, t) = \delta'_{t=0} \mathbf{H}(x), & (x, t) \in \mathbb{R}^d \times \mathbb{R}, \\ \mathbf{u}_0(x, t) = \partial_t \mathbf{u}_0(x, t) = \mathbf{0}, & x \in \mathbb{R}^d, t < 0, \end{cases}$$

and

$$\left\{ \mathbf{g}_0(y, t) = \mathbf{u}_0(y, t), t \in [0, T], y \in \partial\Omega \right\},$$

has been recently addressed in [18, 5, 3]. More precisely, it is proved that the natural imaging functional \mathcal{I} defined by

$$\mathcal{I}[\mathbf{g}_0](x) = \int_0^T \mathbf{v}_s(x, T) ds, \quad x \in \Omega,$$

where the vector field \mathbf{v}_s is defined as the solution of

$$\begin{cases} \partial_t^2 \mathbf{v}_s(x, t) - \mathcal{L}_{\lambda, \mu} \mathbf{v}_s(x, t) = \frac{d\delta_{t=s}}{dt} \mathbf{g}_0(y, T-s) \delta_{y=\partial\Omega}, & (x, t) \in \mathbb{R}^d \times \mathbb{R}, \\ \mathbf{v}_s(x, t) = \partial_t \mathbf{v}_s(x, t) = \mathbf{0}, & x \in \mathbb{R}^d, t < s. \end{cases} \quad (5.1)$$

does not drive to a sufficiently good reconstruction of the source \mathbf{H} . A more efficient reconstruction [5] can then be obtained by considering the following modified version

$$\tilde{\mathcal{I}}[\mathbf{g}_0] = c_s \nabla \times \psi_{\mathcal{I}} + c_p \nabla \phi_{\mathcal{I}}. \quad (5.2)$$

Here $c_p = \sqrt{\lambda + 2\mu}$ and $c_s = \sqrt{\mu}$ denote respectively the pressure and the shear wave speeds and $\psi_{\mathcal{I}}$ and $\phi_{\mathcal{I}}$ represent the compressional and the shear components of \mathcal{I} which is defined from the Helmholtz decomposition of \mathcal{I} :

$$\mathcal{I} = \nabla \times \psi_{\mathcal{I}} + \nabla \phi_{\mathcal{I}}. \quad (5.3)$$

In the sequel, we define respectively the Helmholtz decomposition operator \mathcal{H}^s and \mathcal{H}^p by

$$\mathcal{H}^p[\mathcal{I}] = \nabla \phi_{\mathcal{I}} \quad \text{and} \quad \mathcal{H}^s[\mathcal{I}] = \nabla \times \psi_{\mathcal{I}}.$$

Green function and equivalent Cauchy problem. Let us also introduce the outgoing Green's tensor $\mathbb{G}_{\omega, 0}$ associated to the elastic wave equation

$$(\mathcal{L}_{\lambda, \mu} + \omega^2) \mathbb{G}_{\omega}(x) = -\delta_{\mathbf{x}=\mathbf{0}} \mathbb{I}, \quad x \in \mathbb{R}^d.$$

and \mathbb{G} , the temporal version of the previous Green tensor, defined as the range by the inverse Fourier transform of \mathbb{G}_{ω} , in other words

$$\mathbb{G}(t, \cdot) = \mathcal{F}_t^{-1}[\mathbb{G}_{\omega}(\cdot)](t).$$

Using the same arguments as in the acoustic case, we can show the equivalent of Proposition 2.5.

Proposition 5.1. *For all $t \in [0, s]$, there holds*

$$\begin{cases} \partial_t \mathbb{G}(t, \cdot) &= \partial_t \mathbb{G}(s-t, \cdot) * \partial_t \mathbb{G}(s, \cdot) - \partial_{tt} \mathbb{G}(t, \cdot) * \mathbb{G}(s-t, \cdot) \\ \mathbb{G}(t, \cdot) &= \mathbb{G}(t, \cdot) * \partial_t \mathbb{G}(s-t, \cdot) - \partial_t \mathbb{G}(t, \cdot) * \mathbb{G}(s-t, \cdot) \end{cases} \quad \text{in } \mathcal{D}'(\mathbb{R}^d).$$

In particular, considering $t = 0$, we obtain the identity:

$$\forall s > 0, \quad \delta_{\mathbf{x}=\mathbf{0}} \mathbb{I} = \partial_t \mathbb{G}(s, \cdot) * \partial_t \mathbb{G}(s, \cdot) - \partial_{tt} \mathbb{G}(s, \cdot) * \mathbb{G}(s, \cdot) \quad (5.4)$$

Moreover, the proof of the following theorem follows exactly the same line as the one of Theorem 2.1.

Theorem 5.2. *Let $T_f > 0$, $\varepsilon > 0$, Ω be a connected bounded open set of \mathbb{R}^d and K be a compact set such that $K \subset \Omega$. Then, for all \mathbf{H} such that $\text{supp}(\mathbf{H}^s) \subset K$ and $\text{supp}(\mathbf{H}^p) \subset K$ where \mathbf{H}^s and \mathbf{H}^p are defined from the Helmholtz decomposition of \mathbf{H} :*

$$\mathbf{H}^s = \mathcal{H}^s[\mathbf{H}], \quad \text{and} \quad \mathbf{H}^p = \mathcal{H}^p[\mathbf{H}], \quad (5.5)$$

and for $\varepsilon > 0$ small enough, there exists a Cauchy problem

$$\begin{cases} \partial_t^2 \mathbf{v}_{\varepsilon}(t, x) - \mathcal{L}_{\lambda, \mu} \mathbf{v}_{\varepsilon}(x, t) = \mathbf{0}, & (t, x) \in \mathbb{R}^+ \times \mathbb{R}^d, \\ \mathbf{v}_{\varepsilon}(0, x) = \mathbf{H}_{\varepsilon}(x) \quad \text{and} \quad \partial_t \mathbf{v}_{\varepsilon}(0, x) = \mathbf{G}_{\varepsilon}(x) \end{cases}$$

equivalent to (5.1) in the sense that

$$\mathbf{u}_{\varepsilon}(t, y) = \mathbf{v}_{\varepsilon}(t, y), \quad \forall (t, y) \in [0, T] \times \partial\Omega.$$

Moreover, \mathbf{H}_{ε} and \mathbf{G}_{ε} are given by

$$\mathbf{H}_{\varepsilon} = \mathcal{L}_1[f_{\varepsilon}, \mathbf{H}] = \mathbf{K}_{1, f_{\varepsilon}} * \mathbf{H}, \quad \text{and} \quad \mathbf{G}_{\varepsilon} = \mathcal{L}_2[f_{\varepsilon}, \mathbf{H}] = \mathbf{K}_{2, f_{\varepsilon}} * \mathbf{H},$$

where

$$\mathbf{K}_{1, f_{\varepsilon}}(\cdot) = \int_{\mathbb{R}} f_{\varepsilon}(s) \partial_t \mathbb{G}(s, \cdot) ds \quad \text{and} \quad \mathbf{K}_{2, f_{\varepsilon}}(\cdot) = \int_{\mathbb{R}} f_{\varepsilon}(s) \partial_{tt} \mathbb{G}(s, \cdot) ds,$$

Explicit expression of the associated kernels. The reconstruction of \mathbf{H} from the knowledge of \mathbf{H}_ε can then be performed by using the Helmholtz decomposition of \mathbf{H}_ε as well as two deconvolution procedures. In particular, the explicit expression of each kernel is derived from the proposition below.

Proposition 5.3. *Let $f \in L^2(\mathbb{R})$ be defined from its Fourier transform \hat{f} defined in \mathbb{R}^d by*

$$\hat{f}(\omega) = \sum_{n=0}^{+\infty} \alpha_n \omega^n, \quad \text{with } (\alpha_n)_{n \in \mathbb{N}} \in \ell^2(\mathbb{R}).$$

and let us introduce the four scalar following kernel

$$K_{1,f_\varepsilon}^\alpha(x) = \mathcal{F}_x^{-1} \left[\hat{f}_e(|\xi|c_\alpha\varepsilon) \right] \quad \text{and} \quad K_{2,f_\varepsilon}^\alpha(x) = i\mathcal{F}_x^{-1} \left[\frac{1}{|\xi|} \hat{f}_o(|\xi|c_\alpha\varepsilon) \right], \quad \alpha \in \{s, p\},$$

where f_e and f_o denote respectively the even and odd parts of f . Then we have

$$\mathbf{K}_{1,f_\varepsilon} * \mathbf{H} = K_{1,f_\varepsilon}^p * \mathbf{H}^p + K_{1,f_\varepsilon}^s * \mathbf{H}^s$$

and

$$\mathbf{K}_{2,f_\varepsilon} * \mathbf{H} = K_{2,f_\varepsilon}^p * \mathbf{H}^p + K_{2,f_\varepsilon}^s * \mathbf{H}^s,$$

where \mathbf{H}^p and \mathbf{H}^s are given by (5.5).

The proof of this proposition is essentially based on the Helmholtz decomposition of \mathbb{G}_ω , namely $\mathbb{G}_\omega = \mathbb{G}_\omega^s + \mathbb{G}_\omega^p$ and by remarking that

$$\mathcal{L}_{\lambda,\mu}[\mathbb{G}_\omega^p] = c_p^2 \Delta \mathbb{G}_\omega^p \quad \text{and} \quad \mathcal{L}_{\lambda,\mu}[\mathbb{G}_\omega^s] = c_s^2 \Delta \mathbb{G}_\omega^s.$$

and that for $\alpha \in \{s, p\}$,

$$\int_{\mathbb{R}} (-1)^p \omega^{2p} i \omega \mathbb{G}_\omega^\alpha(\cdot) d\omega = c_\alpha^{2p} \Delta^p (\mathcal{H}^\alpha [\delta_{\{x=0\}} \mathbb{I}]) \quad \text{and} \quad \int_{\mathbb{R}} (-1)^p \omega^{2p} \mathbb{G}_\omega^\alpha(\cdot) d\omega = 0.$$

Finally, the source of \mathbf{H} can be reconstructed by finding separately its compressional and shear components which can be done for instance by using a TV-deconvolution approach :

$$\mathbf{H}^{\alpha,*} = \underset{\mathbf{H}}{\operatorname{argmin}} \{J_\alpha(\mathbf{H})\} \quad \text{with} \quad J_\alpha(\mathbf{H}) = \frac{1}{2} \int_{\Omega} \left(\mathcal{H} \left[\tilde{\mathcal{I}}[\mathbf{g}_\varepsilon] \right]^\alpha - K_{1,f_\varepsilon}^\alpha * \mathbf{H} \right)^2 + \gamma \int_{\Omega} |\nabla \mathbf{H}| dx.$$

6 Comments and conclusion

In this article, we have proposed a systematic method allowing to reconstruct the spatial component of a source term whose temporal component cannot be approximated by a Dirac mass. The proposed algorithm rests upon the use of an imaging technique based on a time reversal approach, and a correction of the reconstructed source with the help of a TV regularization-deconvolution algorithm.

Some first numerical experiment allowed to validate the method in the acoustic framework and we claim that our method is robust enough to be extended to many kinds of wave-like operators involving homogeneous space operators, such as linear elasticity wave ones.

Finally, the approach developed in this article makes a connexion between a regularization in time and in space, where the respective kernels sizes are correlated to the wave velocity.

We are actually investigating the issue of exploiting/generalizing this approach to tackle inverse problems in non-homogenous media where the main unknown is the wave velocity.

References

- [1] H. Ammari. *An Introduction to Mathematics of Emerging Biomedical Imaging*. Mathematics & Applications, Vol. 62, Springer-Verlag, Berlin, 2008.

- [2] H. Ammari, E. Bossy, V. Jugnon, and H. Kang. Mathematical modeling in photoacoustic imaging of small absorbers. *SIAM Rev.*, 52(4):677–695, 2010.
- [3] H. Ammari, E. Bretin, J. Garnier, H. Kang, H. Lee, and A. Wahab. *Mathematical Methods in Elasticity Imaging*. Princeton University Press, Princeton, NJ, USA, 2015.
- [4] H. Ammari, E. Bretin, J. Garnier, and A. Wahab. Time reversal in attenuating acoustic media. In *Mathematical and statistical methods for imaging*, volume 548 of *Contemp. Math.*, pages 151–163. Amer. Math. Soc., Providence, RI, 2011.
- [5] H. Ammari, E. Bretin, J. Garnier, and A. Wahab. Time-reversal algorithms in viscoelastic media. *European J. Appl. Math.*, 24(4):565–600, 2013.
- [6] H. Ammari, E. Bretin, V. Jugnon, and A. Wahab. Photoacoustic imaging for attenuating acoustic media. In *Mathematical modeling in biomedical imaging. II*, volume 2035 of *Lecture Notes in Math.*, pages 57–84. Springer, Heidelberg, 2012.
- [7] H. Ammari, L. G. Bustos, H. Kang, and H. Lee. Transient elasticity imaging and time reversal. *Proceedings of the Royal Society of Edinburgh: Section A Mathematics*, 141(6):1121–1140, 2011.
- [8] H. Ammari, P. Garapon, L. G. Bustos, and H. Kang. Transient anomaly imaging by the acoustic radiation force. *Journal of Differential Equations*, 249(7):1579 – 1595, 2010.
- [9] H. Ammari, P. Garapon, H. Kang, and H. Lee. A method of biological tissues elasticity reconstruction using magnetic resonance elastography measurements. *Quarterly of Applied Mathematics*, 66(1):139–175, 2008.
- [10] G. Bal and K. Ren. Multi-source quantitative photoacoustic tomography in a diffusive regime. *Inverse Problems*, 27(7):075003, 20, 2011.
- [11] G. Bal and G. Uhlmann. Inverse diffusion theory of photoacoustics. *Inverse Problems*, 26(8):085010, 20, 2010.
- [12] C. Bardos and M. Fink. Mathematical foundations of the time reversal mirror. *Asymptot. Anal.*, 29(2):157–182, 2002.
- [13] A. Beck and M. Teboulle. A fast iterative shrinkage-thresholding algorithm for linear inverse problems. *SIAM J. Imaging Sci.*, 2(1):183–202, 2009.
- [14] Z. Belhachmi, T. Glatz, and O. Scherzer. A direct method for photoacoustic tomography with inhomogeneous sound speed. *Inverse Problems*, 32(4):045005, 25, 2016.
- [15] J. Bercoff, M. Tanter, M. Mulle, and M. Fink. The role of viscosity in the impulse diffraction field of elastic waves induced by the acoustic radiation force. *IEEE Trans. Ultrasonics, Ferro., Freq. Control*, 51(6):1523–1536, 2004.
- [16] M. Bergounioux, X. Bonnefond, T. Haberkorn, and Y. Privat. An optimal control problem in photoacoustic tomography. *Math. Models Methods Appl. Sci.*, 24(12):2525–2548, 2014.
- [17] R. I. Brevis, J. H. Ortega, and D. Pardo. A source time reversal method for seismicity induced by mining. *Inverse Probl. Imaging*, 11(1):25–45, 2017.
- [18] S. Catheline, N. Bencech, J. Brum, and C. Negreira. Time reversal of elastic waves in soft solids. *Phys. Rev. Lett.*, 100:064301, Feb 2008.
- [19] A. Chambolle. An algorithm for total variation minimization and applications. *J. Math. Imaging Vision*, 20(1-2):89–97, 2004. Special issue on mathematics and image analysis.
- [20] P. L. Combettes and V. R. Wajs. Signal recovery by proximal forward-backward splitting. *Multiscale Model. Simul.*, 4(4):1168–1200, 2005.
- [21] B. T. Cox, J. G. Laufer, and P. C. Beard. The challenges for quantitative photoacoustic imaging, 2009.

- [22] I. Daubechies, M. Defrise, and C. De Mol. An iterative thresholding algorithm for linear inverse problems with a sparsity constraint. *Comm. Pure Appl. Math.*, 57(11):1413–1457, 2004.
- [23] L. C. Evans. *Partial differential equations*, volume 19 of *Graduate Studies in Mathematics*. American Mathematical Society, Providence, RI, second edition, 2010.
- [24] D. Finch, M. Haltmeier, and Rakesh. Inversion of spherical means and the wave equation in even dimensions. *SIAM J. Appl. Math.*, 68(2):392–412, 2007.
- [25] M. Fink. Time-reversal acoustics. In *Inverse problems, multi-scale analysis and effective medium theory*, volume 408 of *Contemp. Math.*, pages 151–179. Amer. Math. Soc., Providence, RI, 2006.
- [26] J. Greenleaf, M. Fatemi, and M. Insana. Selected methods for imaging elastic properties of biological tissues. *Annual Review of Biomedical Engineering*, 5:57–78, 2003.
- [27] M. Haltmeier, T. Schuster, and O. Scherzer. Filtered backprojection for thermoacoustic computed tomography in spherical geometry. *Math. Methods Appl. Sci.*, 28(16):1919–1937, 2005.
- [28] Y. Hristova. Time reversal in thermoacoustic tomography—an error estimate. *Inverse Problems*, 25(5):055008, 14, 2009.
- [29] Y. Hristova, P. Kuchment, and L. Nguyen. Reconstruction and time reversal in thermoacoustic tomography in acoustically homogeneous and inhomogeneous media. *Inverse Problems*, 24(5):055006, 25, 2008.
- [30] R. Kowar. Integral equation models for thermoacoustic imaging of acoustic dissipative tissue. *Inverse Problems*, 26(9):095005, 18, 2010.
- [31] R. Kowar, O. Scherzer, and X. Bonnefond. Causality analysis of frequency-dependent wave attenuation. *Math. Methods Appl. Sci.*, 34(1):108–124, 2011.
- [32] P. Kuchment and O. Scherzer. *Tomography, Photoacoustic, and Thermoacoustic*, pages 1488–1496. Springer Berlin Heidelberg, Berlin, Heidelberg, 2015.
- [33] L. A. Kunyansky. Explicit inversion formulae for the spherical mean Radon transform. *Inverse Problems*, 23(1):373–383, 2007.
- [34] L. V. Nguyen. A family of inversion formulas in thermoacoustic tomography. *Inverse Probl. Imaging*, 3(4):649–675, 2009.
- [35] G. Paltauf, R. Nuster, M. Haltmeier, and P. Burgholzer. Experimental evaluation of reconstruction algorithms for limited view photoacoustic tomography with line detectors. *Inverse Problems*, 23(6):S81–S94, 2007.
- [36] A. P. Sarvazyan, O. V. Rudenko, S. D. Swanson, J. Fowlkes, and S. Y. Emelianov. Shear wave elasticity imaging: a new ultrasonic technology of medical diagnostics. *Ultrasound in Medicine & Biology*, 24(9):1419 – 1435, 1998.
- [37] O. Scherzer, M. Grasmair, H. Grossauer, M. Haltmeier, and F. Lenzen. *Variational methods in imaging*, volume 167 of *Applied Mathematical Sciences*. Springer, New York, 2009.
- [38] M. Tanter and M. Fink. *Time Reversing Waves For Biomedical Applications*, pages 73–97. Springer Berlin Heidelberg, Berlin, Heidelberg, 2009.
- [39] M. Xu and L. V. Wang. Photoacoustic imaging in biomedicine. *Review of scientific instruments*, 77(4):041101–041101, 2006.